Emerging Protein Targets for Anticancer Metallodrugs: Inhibition of Thioredoxin Reductase and Cathepsin B by Antitumor Ruthenium(II)−Arene Compounds

Angela Casini,[§] Chiara Gabbiani,[§] Francesca Sorrentino,[#] Maria Pia Rigobello,[#] Alberto Bindoli,[‡] Tilmann J. Geldbach,[†] Alessandro Marrone,[⊥] Nazzareno Re,[⊥] Christian G. Hartinger,[†] Paul J. Dyson,[†] and Luigi Messori*[,§]

Department of Chemistry, University of Florence, Via della Lastruccia 3, 50019 Sesto Fiorentino, Firenze, Italy, Department of Biological Chemistry, University of Padova, viale G. Colombo 3, 35121 Padova, Italy, Institute of Neurosciences (CNR), Section of Padova, viale G. Colombo 3, 35121 Padova, Italy, Institut des Sciences et Ingénierie Chimiques, Ecole Polytechnique Fédérale de Lausanne (EPFL), CH-1015 Lausanne, Switzerland, and Dipartimento di Scienze del Farmaco, University G. d'Annunzio, Via dei Vestini 31, 66100 Chieti, Italy

Received June 3, 2008

A series of ruthenium(II)−arene (RAPTA) compounds were evaluated for their ability to inhibit thioredoxin reductase (either cytosolic or mitochondrial) and cathepsin B, two possible targets for anticancer metallodrugs. In general, inhibition of the thioredoxin reductases was lower than that of cathepsin B, although selected compounds were excellent inhibitors of both classes of enzymes in comparison to other metal-based drugs. Some initial structure−activity relationships could be established. On the basis of the obtained data, different mechanisms of binding/inhibition appear to be operative; remarkably the selectivity of the ruthenium compounds toward solid metastatic tumors also correlates to the observed trends. Notably, docking studies of the interactions of representative RAPTA compounds with cathepsin B were performed that provided realistic structures for the resulting protein−metallodrug adducts. Good agreement was generally found between the inhibiting potency of the RAPTA compounds and the computed stability of the corresponding cat B/RAPTA adducts.

Introduction

The field of anticancer metallodrugs is dominated by platinum-based compounds and the so-called "DNA paradigm", which presumes that the mechanism of action of metallodrugs relies on direct DNA damage.[1] However, in recent years, it has become increasingly evident that several cytotoxic metallodrugs exert their biological and pharmacological actions through DNA independent mechanisms.[2] Accordingly, it has become important to delineate these alternative mechanisms and to identify the respective biological targets, as this kind of knowledge might allow a switch to a "molecular targeted" approach of metallodrug design.

Ruthenium(II)−arene pta[a] (pta = 1,3,5-triaza-7-phosphaadamantane) compounds (RAPTA compounds hereafter) are a family of ruthenium(II) compounds of interest as potential antitumor agents: a very favorable biological and pharmacological profile was early established for these compounds.[3] Their mechanism of action is still largely unknown; however, there is evidence that RAPTA compounds work on molecular targets other than DNA,[4] implying a biochemical mode of action profoundly different from classical platinum anticancer drugs. In order to shed some light on their possible molecular mechanism(s), we decided to explore whether RAPTA compounds are able to inhibit two specific enzymes (namely, thioredoxin reductases and cathepsin B) that are believed to be important targets in cancer chemotherapy and are considered to be highly sensitive to metallodrugs (see below).

Thioredoxin reductase (E.C. 1.8.1.9, TrxR) is a ubiquitous flavoenzyme that, together with thioredoxin (Trx) and NADPH, constitutes a critical system for maintaining the cellular redox state.[5,6] Overall, the central functions of the thioredoxin system make it an attractive target for antitumor drug development.[7] Mammalian TrxR is a large homodimer with a glutathione reductase-like structure. Each monomer contains a C-terminal redox center consisting of a cysteine−selenocysteine redox pair that approaches the N-terminal active site of the neighboring subunit for electron transfer.[8]

Notably, the active site selenolate group, after reduction, manifests a large propensity to react with "soft" metal ions, making TrxR a likely pharmacological target for a range of metallodrugs. This hypothesis seems to be valid, as gold(I) and platinum(II) compounds were found to be potent inhibitors of mammalian thioredoxin reductase.[9−12] Interestingly, we recently discovered that a novel (hard) ruthenium(III) "Keppler type" compound acts as moderate inhibitor of rat TrxR.[13]

Cathepsin B (E.C. 3.4.22.1, cat B) is an abundant and ubiquitously expressed cysteine peptidase of the papain family. It is a major component of lysosomal enzymes that is capable of degrading components of the extracellular matrix in diseases such as muscular dystrophy,[14] rheumatoid arthritis,[15] and tumor turnover.[16] Remarkably, cat B turned out to be a prognostic marker for several types of cancer.[17] Increased expression and secretion of cat B have been shown to be causally involved in migration and invasion of numerous human and experimental tumors.[18−20] The exact role of cat B in solid tumors has yet to be defined, but it has been proposed to participate, in connection with other cysteine cathepsins, in metastasis, angiogenesis, and tumor progression.[21−23] Therefore, cat B is a possible therapeutic target for the control of tumor progression, and in this respect, it is not surprising that the use of cat B inhibitors reduces both

* To whom correspondence should be addressed. Phone: +39 055 457 3388. Fax: +39 055 457 3385. E-mail: luigi.messori@unifi.it.
[§] University of Florence.
[#] University of Padova.
[‡] Istituto di Neuroscienze (CNR).
[†] Ecole Polytechnique Fédérale de Lausanne (EPFL).
[⊥] University G. d'Annunzio.

[a] Abbreviations: cat B, cathepsin B; cbdca, 1,1-cyclobutane dicarboxylate; CBZ, *N*-carbobenzoxy; DTNB, 5,5′-dithiobis(2-nitrobenzoic acid); DTT, dithiothreitol; ICP OES, inductively coupled plasma optical emission spectroscopy; pta, 1,3,5-triaza-7-phosphaadamantane; Trx, thioredoxin; TrxR, thioredoxin reductase; TrxR1, cytosolic thioredoxin reductase; TrxR2, mitochondrial thioredoxin reductase.

10.1021/jm8006678 CCC: $40.75
Published on Web 10/04/2008

Chart 1. Chemical Structures of the RAPTA Complexes Used in This Study

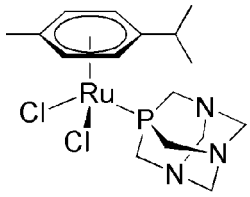

RAPTA-C, **1**

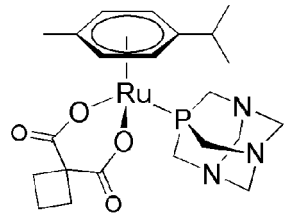

carbo-RAPTA, **2**

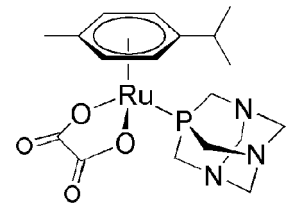

oxalo-RAPTA, **3**

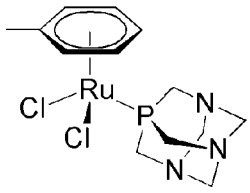

RAPTA-T, **4**

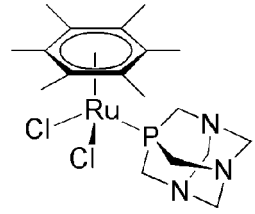

RAPTA-H, **5**

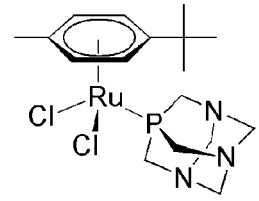

RAPTA-TBMe, **6**

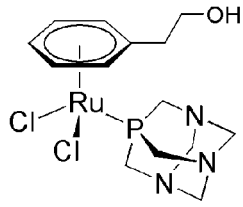

RAPTA-OH, **7**

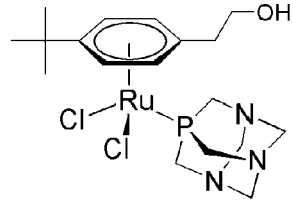

RAPTA-TBOH, **8**

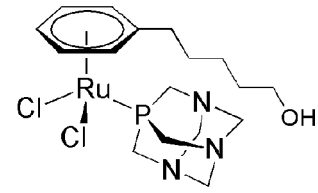

RAPTA-PentaOH, **9**

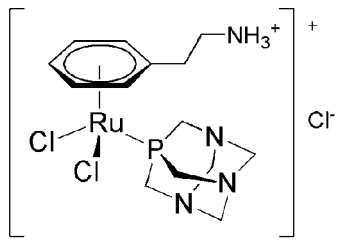

RAPTA-NH_3, **10**

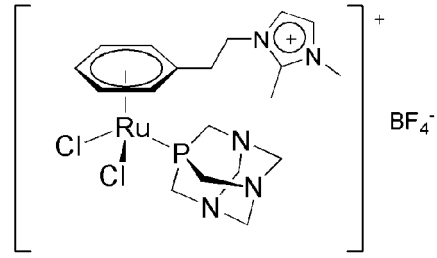

RAPTA-BI, **11**

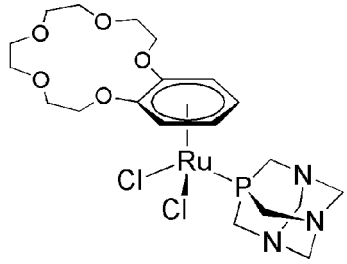

RAPTA-BC, **12**

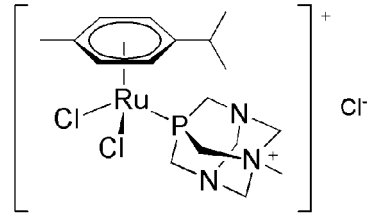

RAPTA-Me^+-C, **13**

tumor cell mobility and invasiveness in vitro.[24] Recently, metal complexes based on rhenium, gold and palladium were shown to be effective inhibitors of cat B.[25−29]

Cathepsin B consists of a light chain (Lys^1-Arg^{49}) and a heavy chain (Val^{50}-Thr^{253})[30] and has seven disulfide bridges;[31] characteristically, bovine cat B has an extra disulfide bond compared with other species such as human and rat. The active site of cat B is formed by an activated Cys and by a His and an Asn residues; near the active site are two main interaction site pockets, a large hydrophobic one and a smaller one, which is more solvent accessible.

The RAPTA compounds studied here are represented in Chart 1, and some of them were recently shown to readily bind to model proteins including ubiquitin, cytochrome *c*, and lysozyme.[32,33] All of the RAPTA compounds share a common structural motif consisting of a ruthenium(II) center bound to an arene and a

Scheme 1. Synthetic Route Used To Prepare **6**, **8**, and **9**[a]

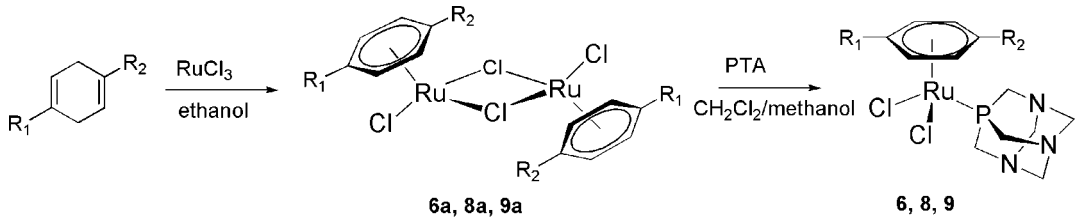

[a] **6**: R_1= CH_3, R_2 = *tert*-butyl. **8**: R_1 = CH_2CH_2OH, R_2 = *tert*-butyl. **9**: R_1 = $C_5H_{10}OH$, R_2 = H.

pta ligand. Notably, the pta group confers water solubility, facilitating administration and transport in the body. Most of the reported compounds differ only in the nature of the arene ligand, although the methylated pta derivative $[RuCl_2(\eta^6\text{-}C_{10}H_{14})(ptaMe)]^+$ **13** (RAPTA-Me^+C) was also included in the study.

For comparison purposes the compounds Ru(η^6-cymene)(pta)($C_6H_6O_4$) **2** (carbo-RAPTA) and Ru(η^6-cymene)(pta)(C_2O_4) **3** (oxalo-RAPTA) were also investigated. Replacement of the two chlorides with the stronger bidentate ligands (oxalate or cyclobutane dicarboxylate) greatly reduces the rate of aquation, thus modifying the overall solution behavior without adversely affecting cytotoxicity.[34]

The 13 investigated compounds manifest a similar cell-growth inhibition activity against a number of representative cancer cell lines (HT29 colon carcinoma, the A549 lung carcinoma, and the T47D and MCF7 breast carcinoma), and in general the in vitro cytotoxicity is low. Nevertheless, excellent antimetastatic and pharmacokinetic properties were observed in vivo for several RAPTA compounds,[3] similar to those reported for NAMI-A, a drug that failed the NCI screening program but successfully completed phase I clinical trials.[35,36]

The binding of a wide range of RAPTA derivatives to oligonucleotides was studied in detail, but no direct correlation between oligonucleotide binding and cytotoxicity could be observed.[37,38] This finding might suggest that other protein targets are of greater importance in producing the observed cytotoxic effects. Thus, TrxR and cat B may represent potential targets for this novel class of ruthenium compounds and the inhibition of these enzymes by RAPTA compounds is discussed herein. In addition, in the case of cat B, modeling studies were able to provide highly reliable molecular structures of selected RAPTA−protein adducts.

Results and Discussion

The RAPTA compounds shown in Chart 1 were prepared as described previously (see Experimental Section) with the exception of **6**, **8**, and **9**, which were prepared in a two step process commencing with the appropriate diene obtained from Birch reduction (see Scheme 1 and Experimental Section for further details).

Spectroscopic data of **6**, **8**, and **9** corroborated the proposed structures. Of note, the ^{31}P NMR spectra of **6**, **8**, and **9** in DMSO-d_6 exhibit a singlet resonance around −31 ppm, which is typical for the RAPTA structural motif.[38] The structure of **9** has been established in the solid state by single crystal X-ray diffraction analysis and is shown in Figure 1 with key bond parameters provided in the caption.

The structure of **9** comprises the expected piano-stool geometry characteristic of RAPTA compounds with bond lengths and angles around the metal center, in good agreement with those reported earlier for comparable molecules.[42] The crystallographic unit cell contains two independent molecules

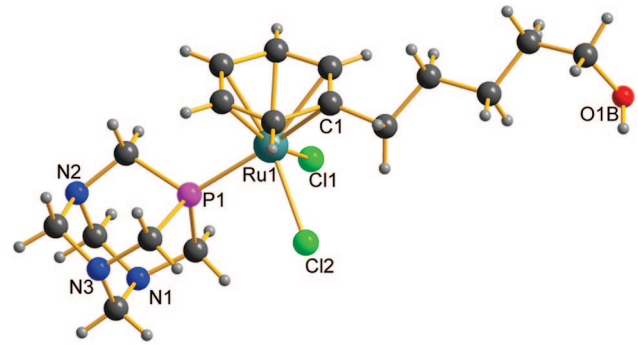

Figure 1. Ball-and-stick representation of the molecular structure of **9**. Key bond lengths (Å) and angles (deg) include the following: Ru(1)−Cl(1), 2.430(1); Ru(1)−Cl(2), 2.422(1); Ru(1)−P(1), 2.305(2); Ru(1)−C(1), 2.317(5); Cl(1)−Ru(1)−Cl(2), 87.63(5); Cl(1)−Ru(1)−P(1), 86.86(5); P(1)−Ru(1)−Cl(2), 83.62(5).

Table 1. IC_{50} (μM) of **1**−**13** against TrxR1 and TrxR2

compd	TrxR1 IC_{50} (μM)	TrxR2 IC_{50} (μM)
1 RAPTA-C	37.1 ± 1.2	>200
2 carbo-RAPTA	4.6 ± 0.5	14.7 ± 1.5
3 oxalo-RAPTA	32.5 ± 1.2	100
4 RAPTA-T	144 ± 4.5	>200
5 RAPTA-H	>200	>200
6 RAPTA-TBMe	82.2 ± 3.1	200
7 RAPTA-OH	80 ± 10.4	>200
8 RAPTA-TBOH	24.5 ± 2.1	>200
9 RAPTA-pentaOH	>200	>200
10 RAPTA-NH_3	49.4 ± 2.5	>200
11 RAPTA-BI	>200	>200
12 RAPTA-BC	>200	>200
13 RAPTA- Me^+C	100	>200
1,1-cyclobutanedicarboxylate	>200	>200

(of which one is shown in Figure 1), and because the pentane-1-ol sidearm is disordered (see Experimental Section), the bond parameters are not described in detail.

Thioredoxin Reductase Inhibition. The in vitro data for rat TrxR inhibition by **1**−**13** are summarized in Table 1, with all RAPTA compounds being tested against both cytosolic and mitochondrial thioredoxin reductase. Typically, inhibition of the mitochondrial form is low, whereas in all cases, inhibition of cytosolic thioredoxin reductase is more pronounced. This finding is in agreement with a previous study showing that ruthenium compounds are more effective inhibitors of the cytosolic form of TrxR compared to the mitochondrial form.[13] Moreover, it is evident that inhibition of cytosolic thioredoxin reductase varies significantly through the various RAPTAs with IC_{50} values ranging from 4 μM to more than 200 μM. Notably, carbo-RAPTA **2** is the most effective inhibitor, being about 10-fold more efficient than the prototype compound RAPTA-C **1** (Chart 1); this finding implies that **2** retains its 1,1-cyclobutandicarboxylate (cbdca) ligand when interacting with TrxR because the arene ligand in the two compounds is the same, i.e., *p*-cymene. It is worth noting that 1,1-cyclobutandicarboxylic

Table 2. IC_{50} (μM) of **1**−**13** against bovine cat B

compd	cat B IC_{50} (μM)
1 RAPTA-C	2.5 ± 0.5
2 carbo-RAPTA	5 ± 0.6
3 oxalo-RAPTA	>200
4 RAPTA-T	1.5 ± 0.2
5 RAPTA-H	>200
6 RAPTA-TBMe	82 ± 3.1
7 RAPTA-OH	1.6 ± 0.4
8 RAPTA-TBOH	24.5 ± 2.1
9 RAPTA-pentaOH	7 ± 0.8
10 RAPTA-NH_3	13 ± 3.0
11 RAPTA-BI	>100
12 RAPTA-BC	5 ± 0.5
13 RAPTA-Me^+C	6.5 ± 0.4

acid (the precursor to the ligand) is not a TrxR inhibitor (IC_{50} > 200 μM, in Table 1). Moreover, it was earlier reported that loss of the cbdca ligand from **2** is very slow, leading to a substantial reduction of covalent adduct formation with model proteins.[33] Combined, these observations suggest that TrxR forms a relatively tight adduct with unmodified carbo-RAPTA and that this adduct is specifically stabilized by interactions occurring between the cbdca moiety and the protein itself.

From inspection of the data it is also evident that as the steric demand of the arene ligand increases, a net decrease of thioredoxin reductase inhibition is observed (see as examples **5**, **11**, and **12**). This observation implies that the protein cannot easily accommodate arene ligands that have bulky substituents. It has previously been shown by mass spectrometric methods that the arene is not lost from the RAPTA structure on protein binding. Instead, cleavage of the metal−chloride bonds is observed, in some cases followed by subsequent loss of the pta ligand.[32]

Cathepsin B Inhibition. The in vitro data for cat B inhibition of **1**−**13** are reported in Table 2, revealing that the different complexes inhibit cathepsin B to varying degrees. The most effective compounds in the series are RAPTA-T **4** (IC_{50} = 1.5 ± 0.2 μM) and RAPTA-OH **7** (IC_{50} = 1.6 ± 0.4 μM), followed by RAPTA-C **1** (IC_{50} = 2.5 ± 0.5 μM), RAPTA-BC **12** (IC_{50} = 5 ± 0.5 μM), and RAPTA-pentaOH **9** (IC_{50} = 7 ± 0.8 μM). Indeed, **4** is the most active RAPTA compound of those tested in vivo, with a selective mode of action toward metastasis, which could indicate that cat B is a possible target for RAPTA complexes in vivo.

Previously it has been shown that positively charged groups can enhance the inhibition activity of complexes toward cat B, whereas RAPTA-NH_3 **10** and RAPTA-BI **11** (which are both cationic) are actually less effective inhibitors with IC_{50} values of 13 and ∼100 μM, respectively. However, it must be noted that hydrolysis of all compounds renders them cationic.

Compounds RAPTA-OH **7** and RAPTA-TBOH **8** (in **8** a *tert*-butyl group is present with respect to **7**, in order to modify the hydrophobicity of the complex) exhibit comparatively low activities (IC_{50} = 18 ± 3 μM) possibly because of the steric hindrance of the larger arene ring, which might decrease the accessibility of the ruthenium center toward the thiolates in the active site. It is also worth noting here that the dichloro complex RAPTA-C **1** is more active than the dicarboxylate analogues carbo-RAPTA **2** (IC_{50} = 5 ± 0.6 μM) and oxalo-RAPTA **3** (IC_{50} ≈ 200 μM). This difference might be due to the fact that initial hydrolysis, followed by covalent binding to cat B, is required for effective inhibition, although a direct, associative ligand substitution mechanism cannot be entirely ruled out.[39]

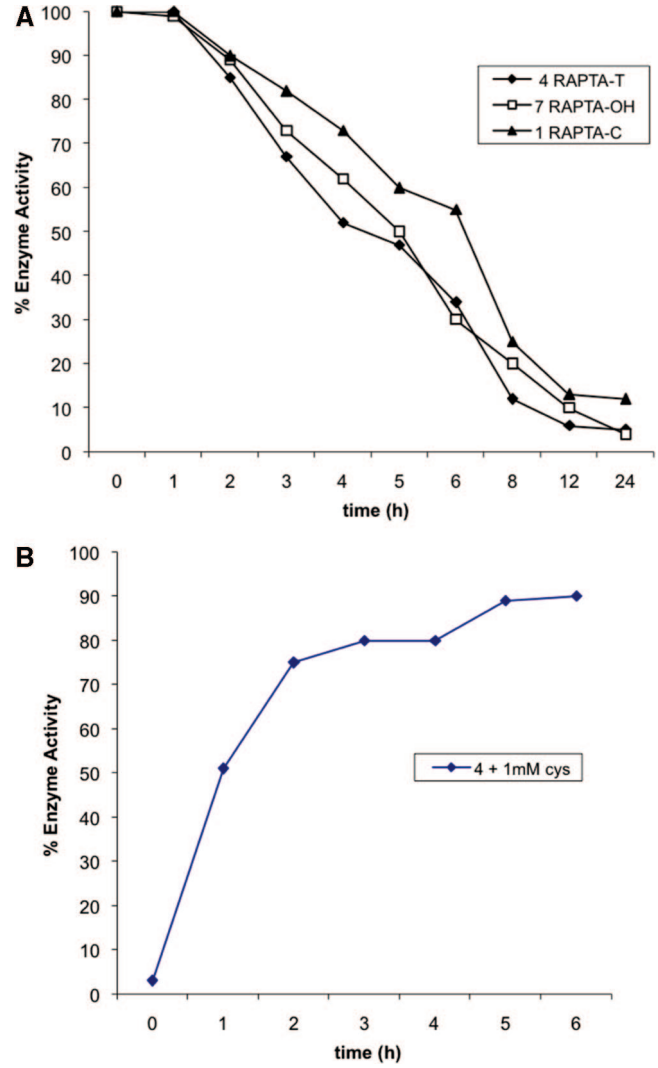

Figure 2. (A) Time-dependent inhibition of cat B by 5 μM **1**, **4**, and **7**. (B) Cysteine reactivation of cat B inhibited by 5 μM **4**.

The nontumor selective (and naturally cationic) compound RAPTA-Me^+C **13** shows a reduced IC_{50} (6.5 ± 0.4 μM) with respect to **1**.

Examination of the inhibition of cat B by RAPTA-OH **7**, RAPTA-T **4**, and RAPTA-C **1** over time revealed an exponential decay of enzyme activity (Figure 2A). This is the typical inhibition pattern of time-dependent inhibitors, where a finite period of time is required to establish maximum inhibition (12 h here), after which time no further inhibition is obtained. The time dependence and cysteine reactivation properties were evaluated for **1**, **4**, and **7** in order to characterize the reversibility of inhibition. It was found that addition of 1 mM cysteine results in full recovery of activity within 6 h. Figure 2B reports the cysteine reactivation data for **4**.

Structural Inferences on the Resulting Metallodrug/Protein Hybrids. Analysis of the enzyme inhibition data described above allows drawing of precise structural inferences for the resulting metallodrug/protein adducts to be inferred. In the case of cytosolic thioredoxin reductases it can be proposed that the various RAPTA compounds retain the arene ligands upon binding the enzyme. Notably, the presence of bulky substituents on the arene greatly reduces enzyme inhibition. It is noteworthy that carbo-RAPTA **2** is a more effective inhibitor than RAPTA-C **1**, which implies that the cbdca ligand remains bound to the ruthenium when forming the initial protein adduct.

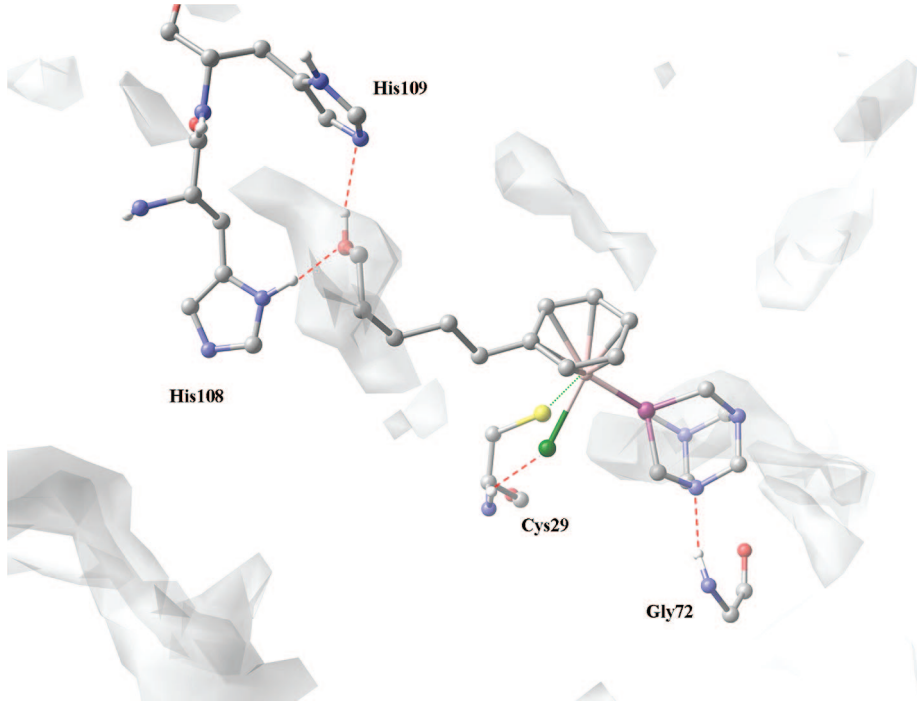

Figure 3. Docking geometry of **9** to Cat B illustrating the main interactions of the ligand with the residues flanking the active site. Also shown in "transparent" rendering is the contour map for the hydrophobic field, calculated with the side-map module implemented in Maestro.

A similar inference has been implied from another study involving diketonate derivatives of **1**.[40]

A different inhibition mechanism appears to be involved in the case of cat B in that **1** is far more effective than **2**; this observation suggests that the release of the leaving group is important for activity. The most inert complex (at least in terms of hydrolysis and subsequent ligand exchange) is oxalo-RAPTA **3**. Accordingly, inhibition of cat B is presumably related to coordination of the ruthenium(II) center to a protein residue in the active site. It is likely that the active site cysteine is the effective anchoring site for RAPTA upon consideration of the soft character of the ruthenium center. This hypothesis was supported by specific docking studies (see next paragraph). It also emerges that ruthenium binding to cat B is largely modulated by the nature of the arene ligand. Bulky groups on the arene ligand reduce the binding affinity (compare **5** and **6** with **4** and compare **8** and **9** with **7**). A positive charge on the arene also reduces affinity (compare **10** with **7**). Surprisingly, **12** is still very effective despite the presence of a bulky crown ether substituent on the arene ligand.

Docking Studies. Molecular docking studies have been successfully employed in rational drug design, but they have not been widely applied to study metal complexes. Although several docking programs, such as Gold, can tackle metal centers, it usually corresponds to part of a cofactor or an enzyme active site. Only a limited number of docking studies have been performed so far where the metal center is incorporated into the ligand being docked.[41,42]

Herein, docking studies were performed to investigate the possible binding modes of the RAPTA complexes and to facilitate the elucidation of structure−activity relationships. We have limited our attention to cat B, as its inhibition is far more pronounced and shows a clear modulation according to the nature of the arene ligand. In addition, the binding site for ruthenium complexes in cat B is well established.

Six of the RAPTA compounds were considered in the study, i.e., **1**, **4**, **5**, **6**, **7**, and **9**, which span a wide range of IC_{50} values

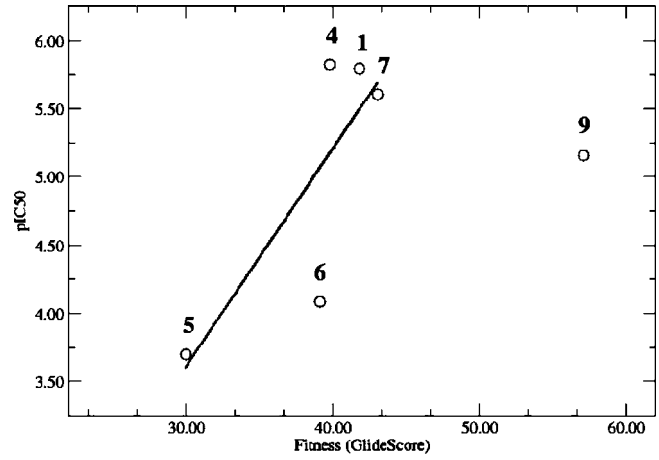

Figure 4. Correlation between calculated GoldScore and experimental activities (pIC_{50}) of the inhibitors. Compound **9** (on the right) has not been included in the correlation (see main text).

and are representative of the homogeneous class of neutral dichloride complexes. We assumed that inhibition is preceded by aquation of one labile chloride ligand and implies subsequent coordination of the ruthenium(II) center to the active site cysteine residue, which acts as the common anchoring site for all these Ru(II) complexes. For each of the complexes, both possible configurations corresponding to aquation of either of the two chloride ligands were independently considered and only the best docked pose was kept.

Although the docking mode of the active compounds depends on the particular complex being docked, in all successful dockings the ligand had a favorable interaction with at least some of the surrounding residues besides Cys29. This is exemplified by the docking mode of **9**, illustrated in Figure 3, which shows close interactions with residues Gly72 (hydrogen bond to a nitrogen atom of the PTA ligand) and His108 and His109 (hydrogen bonds to hydroxyl group on the arene ligand). In addition, the remaining chloride ligand interacts with the

backbone amide nitrogens of Cys29 in which the side chain sulfur atom coordinates the ruthenium center, and the alkyl and aryl portions of the coordinated ligands find favorable interaction with hydrophobic sites of the protein. It is worth noting that the pta ligand sits in the pocket occupied by a conserved water molecule in the native protein, finding several favorable hydrophobic interactions beyond the hydrogen bond with Gly72.

From the docking calculations, a Goldscore value for each inhibitor was calculated and compared with the corresponding experimental inhibitory IC_{50} activities. The experimental pIC_{50} values were plotted against the calculated docking scores, showing in all cases a satisfactory correlation, with the exception of **9** where the activity is overestimated by the docking procedure. The exclusion of this compound significantly improves the correlation, leading to correlation coefficient $R^2 = 0.64$ (Figure 4).

Conclusions

RAPTA compounds are novel ruthenium compounds with a very encouraging pharmacological profile. There is now enough evidence to suggest that their mechanism of action is DNA-independent and substantially different from cisplatin and related anticancer platinum drugs. This prompted us to explore their interactions with potential new targets and focused our attention on protein targets, as a significant reactivity of RAPTA compounds with model proteins was recently highlighted. In particular, we have explored here their reactivity against two emerging protein targets for anticancer metallodrugs, namely, thioredoxin reductase and cathepsin B.

RAPTA compounds behave as rather potent inhibitors of cathepsin B, whereas inhibition of thioredoxin reductase is far less pronounced (with the only exception of **2**). On average, IC_{50} values in the low micromolar range were measured for cat B inhibition, whereas in the case of cytosolic thioredoxin reductase, IC_{50} values fall in the 45−200 μM range. These results imply that RAPTA compounds might be effective inhibitors of cat B at physiologically attainable concentrations while inhibition of thioredoxin reductase seems to be modest and scarcely relevant. These data matche in vivo data well, which shows that RAPTA compounds reduce the mass and number of metastasis with cat B being primarily implicated in the process of metastasis.

When the interaction of RAPTA compounds with cat B is considered, it emerges that IC_{50} values are spread over a rather wide range, and there is indeed a strong modulation of cat B inhibition by the nature of the arene ligand. A detailed analysis of the enzyme inhibition data for the 13 tested RAPTA compounds allowed us to establish structural inferences on the nature of the resulting metallodrug−protein adducts. It is likely that RAPTA compounds, upon binding to either TrxR or cat B, retain the arene ligand, and therefore, the measured IC_{50} values show a marked dependence on the nature of the latter. The chloride ligands are instead labile ligands and undergo facile aquation, albeit highly dependent on the conditions, e.g., free chloride concentration, pH, compound concentration, etc. In two cases the chloride ligands were replaced by dicarboxylate ligands that are far more inert. Analyses of IC_{50} values for these compounds favor the idea that the dicarboxylate ligands are retained when forming the adduct with TrxR1. In contrast, release of the dicarboxylate appears to be required to bind and inhibit cat B. Active site cysteine is proposed to be the anchoring site for the ruthenium(II) center when RAPTAs bind to cat B.

Finally, docking studies of the interactions of six representative RAPTA compounds with cat B were carried out that produced reliable structures for the resulting protein−metallodrug adducts. Beyond the coordinative bond of ruthenium(II) to the sulfur of the active site cysteine, a number of additional contacts of the docked RAPTAs with the protein surface residues were highlighted that further stabilized these adducts. Overall, a satisfactory agreement was found between the cat B inhibiting potency of the considered RAPTA compounds and the stability of the corresponding cat B−RAPTA adducts.

Experimental Section

Synthesis of the Compounds. The starting material 1,3,5-triaza-7-phosphaadamantane (pta)[43] and complexes **1**−**5**, **7**, and **10**−**13**[3,34,38,44] were prepared as described previously. Reactions were carried out under nitrogen atmosphere, and solvents were purged with nitrogen before use. ^{1}H, ^{13}C, and ^{31}P NMR spectra were recorded on a Bruker 400 MHz Ultrashield spectrometer. Electrospray ionization mass spectra (ESI-MS) were obtained on a Thermo Finnigan LCQ Deca XP Plus quadrupole ion trap instrument set in positive mode using a literature method.[45]

Synthesis of the Dimeric Precursors 6a, 8a, and 9a. A suspension of $RuCl_3$ together with an excess of the diene (3.5 equiv, obtained from the appropriate arene by Birch reduction) was stirred at reflux for 12 h, affording a red solution and a dark-brown residue. The mixture was filtered while hot and the clear red filtrate stored at −20 °C, resulting in the precipitation of an orange microcrystalline solid, which was isolated by filtration and washed with diethyl ether, affording the product.

6a. Yield: 79%. ^{1}H NMR (DMSO-d_6, 400 MHz): 6.05 (d, $^3J_{HH}$ = 6.4, 4H, H_{arene}), 5.74 (d, $^3J_{HH}$ = 6.4, 4H, H_{arene}), 2.09 (s, 6H, H_{methyl}), 1.35 (s, 18H, $H_{t\text{-}butyl}$). ^{13}C NMR (DMSO-d_6, 100 MHz): 109.8 (C_{arene}), 101.0 (C_{arene}), 85.6 (C_{arene}), 85.4 (C_{arene}), 34.7 ($C_{t\text{-}buyl}$), 30.3 ($C_{t\text{-}buyl}$), 18.4 (C_{methyl}).

8a. Yield: 86%. ^{1}H NMR (DMSO-d_6, 400 MHz): 6.06 (d, $^3J_{HH}$ = 6.4, 4H, H_{arene}), 5.80 (d, $^3J_{HH}$ = 6.4, 4H, H_{arene}), 3.67 (t, $^3J_{HH}$ = 6.0, 4H, H_{ethyl}), 2.52 (t, $^3J_{HH}$ = 6.0, 4H, H_{ethyl}), 1.36 (s, 18H, $H_{t\text{-}butyl}$). ^{13}C NMR (DMSO-d_6, 100 MHz): 111.0 (C_{arene}), 100.6 (C_{arene}), 86.9 (C_{arene}), 84.4 (C_{arene}), 60.5 (C_{ethyl}), 36.1 (C_{ethyl}), 34.9 ($C_{t\text{-}butyl}$), 30.3 ($C_{t\text{-}butyl}$).

9a. Yield: 74%. ^{1}H NMR (DMSO-d_6, 400 MHz): 5.98 (dd, $^3J_{HH}$ = 5.6, $^3J_{HH}$ = 6.0, 4H, H_{arene}), 5.75 (d, $^3J_{HH}$ = 6.0, 4H, H_{arene}), 5.73 (t, $^3J_{HH}$ = 5.6, 2H, H_{arene}), 4.37 (s, br, 2H, O*H*), 3.39 (t, $^3J_{HH}$ = 6.0, 4H, H_{pentyl}), 2.44 (t, $^3J_{HH}$ = 8.0, 4H, H_{pentyl}), 1.59 (tt, 4H, H_{pentyl}), 1.46 (tt, 4H, H_{pentyl}), 1.41 (tt, 4H, H_{pentyl}). ^{13}C NMR (DMSO-d_6, 100 MHz): 108.5 (C_{arene}), 89.5 (C_{arene}), 85.2 (C_{arene}), 83.4 (C_{arene}), 61.0 (C_{pentyl}), 33.1 (C_{pentyl}), 32.7 (C_{pentyl}), 29.2 (C_{pentyl}), 25.7 (C_{pentyl}).

Synthesis of 6, 8, and 9. To a solution of the ruthenium dimer in 1:1 CH_2Cl_2/MeOH, pta (2.05 equiv) was added, and the mixture was stirred for 40 min at room temperature. The solvent of the resulting orange-red solution was removed in vacuo and the remaining solid washed with Et_2O to afford the product as orange powder.

6. Yield: 88%. ^{1}H NMR (DMSO-d_6, 400 MHz): 6.00 (d, $^3J_{HH}$ = 6.0, 2H, H_{arene}), 5.76 (d, $^3J_{HH}$ = 6.0, 2H, H_{arene}), 4.48 (s, br, 6H, H_{PTA}), 4.19 (br, s, 6H, H_{PTA}), 1.87 (s, 3H, H_{methyl}), 1.25 (s, 9H, $H_{t\text{-}butyl}$). ^{13}C NMR (DMSO-d_6, 100 MHz): 107.8 (C_{arene}), 94.6 (C_{arene}), 88.2 (d, $^2J_{PC}$ = 5, C_{arene}), 84.3 (d, $^2J_{PC}$ = 5, C_{arene}), 72.4 (d, $^3J_{CP}$ = 6, C_{PTA}), 51.8 (d, $^1J_{CP}$ = 17, C_{PTA}), 34.4 ($C_{t\text{-}butyl}$), 30.3 ($C_{t\text{-}butyl}$), 18.4 (C_{methyl}). ^{31}P NMR (DMSO-d_6, 162 MHz): −31.8 (s). MS (ESI, H_2O): 442.1 $[M - Cl]^+$. Anal. Calcd for $C_{17}H_{28}Cl_2N_3PRu$ (477.37 g/mol): C, 42.77; H, 5.91; N, 8.80. Found: C, 41.08; H, 5.64; N, 8.53.

8. Yield: 87%. ^{1}H NMR (DMSO-d_6, 400 MHz): 6.14 (d, $^3J_{HH}$ = 6.0, 2H, H_{arene}), 5.96 (d, $^3J_{HH}$ = 6.0, 2H, H_{arene}), 4.78 (m, 6H, H_{PTA}), 4.30 (dd, $^2J_{PH}$ = 39, d, $^2J_{PC}$ = 5, 6H, H_{PTA}), 3.61 (t, $^3J_{HH}$ = 6.0, 2H, H_{ethyl}), 2.27 (t, $^3J_{HH}$ = 6.0, 2H, H_{ethyl}), 1.26 (s, 9H, $H_{t\text{-}butyl}$). ^{13}C NMR (DMSO-d_6, 100 MHz): 109.4 (C_{arene}), 96.9 (C_{arene}), 89.0 (d, $^2J_{PC}$ = 5, C_{arene}), 84.8 (d, $^2J_{PC}$ = 6, C_{arene}), 70.6 (d, $^2J_{PC}$ = 5, C_{PTA}), 60.6 (C_{ethyl}), 49.0 (d, $^2J_{PC}$ = 17, C_{PTA}), 36.3 (C_{ethyl}), 34.5 ($C_{t\text{-}butyl}$), 30.3 ($C_{t\text{-}butyl}$). ^{31}P NMR (DMSO-d_6, 162

Table 3. Crystallographic Data for **9**

formula	$C_{17}H_{28}Cl_2N_3OPRu$
M	493.36
T (K)	140(2)
crystal system	monoclinic
space group	*Pn*
a (Å)	6.6343(13)
b (Å)	20.033(4)
c [Å]	15.188(3)
α (deg)	90
β (deg)	97.73(3)
γ(deg)	90
V (Å^3)	2000.2(7)
Z	4
density [Mg/m^3]	1.638
μ [mm^{-1}]	1.142
2Θ range (deg)	$3.21 \leq 2\Theta \leq 25.03°$
reflections collected	26957
independent reflections	6877 ($R_{int} = 0.0565$)
GOF on F^2	1.091
final R1, wR2 ($I > 2\sigma(I)$)	0.0354, 0.0610

MHz): −31.9 (s). Anal. Calcd for $C_{18}H_{30}Cl_2N_3OPRu$ (507.4 g/mol): C, 42.61; H, 5.96; N, 8.28. Found: C, 39.73; H, 5.54; N, 7.91.

9. Yield: 93%. ^{1}H NMR (DMSO-d_6, 400 MHz): 5.78 (dd, br, 1H, H_{arene}), 5.59 (d, $^3J_{HH} = 6.0$, 2H, H_{arene}), 5.31 (t, $^3J_{HH} = 5.6$, 1H, H_{arene}), 4.43 (br, 6H, H_{PTA}), 4.38 (t, $^3J_{HH} = 5.2$, 1H, O*H*), 4.18 (br, 6H, H_{PTA}), 3.38 (m, 2H, H_{pentyl}), 2.29 (t, $^3J_{HH} = 7.6$, 2H, H_{pentyl}), 1.55 (tt, 2H, H_{pentyl}), 1.44 (tt, 2H, H_{pentyl}), 1.35 (tt, 2H, H_{pentyl}). ^{13}C NMR (DMSO-d_6, 100 MHz): 109.6 (d, $^2J_{CP} = 4$, C_{arene}), 87.0 (d, $^2J_{CP} = 6$, C_{arene}), 86.5 (d, $^2J_{CP} = 2$, C_{arene}), 77.9 (C_{arene}), 72.7 (d, $^3J_{CP} = 7$, C_{PTA}), 61.0 (C_{pentyl}), 52.3 (d, $^1J_{CP} = 17$, C_{PTA}), 32.8 (C_{pentyl}), 31.4 (C_{pentyl}), 29.2 (C_{pentyl}), 25.7 (C_{pentyl}). ^{31}P NMR (DMSO-d_6, 162 MHz): −31.9 (s). MS (ESI, H_2O): 458.1 $[M - Cl]^+$. Anal. Calcd for $C_{17}H_{28}Cl_2N_3PORu$ (493.37 g/mol): C, 41.39; H, 5.72; N, 8.52. Found: C, 41.09; H, 6.04; N, 8.55.

Crystallography. Crystals suitable for X-ray diffraction were obtained by slow diffusion of diethyl ether into an ethanol solution of **9**. Data collection for the X-ray structure determination was performed on a Bruker Nonius ApexII CCD diffractometer system using graphite-monochromated Mo Kα (0.71070 Å) radiation and a low temperature device ($T = 140(2)$ K). Data reduction was performed by EvalCCD and the structure solved and refined with SHELX97.[46] The graphical representation of the structure was made with Diamond.[47] The structure was solved by direct methods and successive interpretation of the difference Fourier maps, followed by full matrix least-squares refinement (against F^2). Atoms were refined anisotropically, and the contribution of the hydrogen atoms, in their calculated positions, was included in the refinement using a riding model. The unit cell contains two independent molecules, both displaying disorder in the pentol side chain. Carbon atoms in the side chain were split over two positions and constrained using the DFIX command. Relevant crystallographic data are compiled in Table 3.

Enzyme Inhibition Assays. Thioredoxin Reductase. Highly purified cytosolic thioredoxin reductase (TrxR1) was obtained from rat liver according to Luthman and Holmgren,[48] and mitochondrial thioredoxin reductase (TrxR2) was purified starting from isolated mitochondria according to Rigobello et al.[49] Proteins of the purified isoforms of thioredoxin reductases were assayed with the procedure of Lowry et al.[50]

The ruthenium complexes, at the indicated concentrations, were preincubated at 25 °C for 30 min in 0.2 M Na, K-phosphate buffer (pH 7.5) containing 5 mM EDTA. Afterward, TrxR1 (1.5 (*μ*g of protein)·mL^{-1}) or TrxR2 (4 (*μ*g of protein)·mL^{-1}) was added, together with 0.3 mM NADPH, and after another 5 min of incubation the reaction was started by the addition of 1.5 mM DTNB to both sample and reference cuvettes. The increase in optical density at 412 nm was monitored for ∼20 min. Results are indicated as percentage of activity with respect to the control and reported versus the respective concentrations in order to obtain the reported IC_{50} values. Specific activities of the noninhibited reaction were 12 *μ*mol min^{-1} mg^{-1} protein for TrxR1 and 5.4 *μ*mol min^{-1} mg^{-1} protein for TrxR2.

Cathepsin B. Crude bovine spleen cat B was purchased from Sigma (C6286) and used without further purification. The colorimetric cat B assay was performed in 100 mM sodium phosphate, 1 mM EDTA, 0.025% polyoxyethylene (23) lauryl ether (BRIJ), pH 6.0, using Na-CBZ-L-lysine *p*-nitrophenyl ester (CBZ = *N*-carbobenzoxy) as substrate. For the enzyme to be catalytically functional, the active site cysteine needs to be in a reduced form. Therefore, prior to use, cat B was prereduced with dithiothreitol (DTT) to ensure that the majority of the enzyme is in a catalytically active form. Thus, cat B was activated, before dilution, in the presence of excess DTT for 1 h at 30 °C.

IC_{50} determinations were performed in triplicate using a fixed enzyme concentration of 500 nM and a fixed substrate concentration of 200 *μ*M. Inhibitor concentrations ranged from 0.3 to 200 *μ*M. The enzyme and inhibitor were co-incubated at 30 °C over a period of 24 h prior to the addition of substrate. Activity was measured over 3 min at 326 nm. Colorimetric readings were performed on a Lambda 20 Bio spectrophotometer (Perkin-Elmer).

Cysteine reactivation was evaluated using an inhibitor concentration of approximately the IC_{50} up to 5 IC_{50}, depending on the potency of the inhibitor. The enzyme−inhibitor incubation times for the cysteine reactivation assay were 1, 2, 3, 4, 5, and 6 h after an initial 24 h incubation with the compound at 30 °C. After the initial incubation, 1 mM cysteine was added, and incubation was continued for the required time at 30 °C. Following incubation, substrate was added and activity was read.

Computational Models and Methods. The crystal structures of cat B in the apo form, and covalently bound to 5-mercaptopyridine (1IPP) and an epoxide substrate (1CSB), were obtained from the PDB archives. The retrieved PDB entries were superimposed and graphically inspected using the molecular modeling software Maestro 7.0.[51] This preliminary analysis showed that the cathepsin binding site does not significantly change in the bound or native forms, and we therefore decided to investigate the binding properties of the RAPTA complexes by employing 1IPP to model the structure of the cat B binding site.

The protein structure employed in the docking calculations was obtained using the Protein Preparation module implemented in the Maestro graphical interface. This procedure is used to obtain an all-atom force field consistent protein structure from the corresponding PDB structure by essentially adding hydrogen atoms, removing the cocrystallized water molecules, and setting the ionizable residues in the form expected at physiological pH. In particular, the Cys29 and the His119 residues, within the active site, were set in the ionized forms.

The structures of the RAPTA complexes were drawn with Maestro 7.0 and subsequently optimized through DFT calculations at the B3LYP/LACVP** level of theory [52,53] using the Jaguar suite of programs.[54]

Among the several possible conformations originated by rotation of the arene ring around the metal−centroid bond, we considered only those with the most hindered benzene substituent, namely, the $(CH_2)_nOH$ in **7** and **9** and isopropyl in **5**, at the maximum distance from the pta ligand. This choice corresponds to the most stable conformation and allows the extended conformations of these ligands to be obtained and, from a graphical inspection, to better fit the cat B binding site.

The complexes minimized with the above DFT procedure were docked into the cat B binding site by means of Gold 3.0.1.[55] The region of interest used by Gold was defined as a 15 Å sphere around the Cys29 sulfur atom. Metal coordination in GOLD is modeled as "pseudohydrogen bonding" in which the metals can be considered to bind to H-bond acceptors and the metal will compete with the H-bond donors for interaction. The ruthenium ion was set as a tetrahedral atom; the docking program recognized the coordination of the chloride, the pta, and the arene ligands, and then in order to satisfy the pseudotetrahedral geometry, the missing coordination position was used as a fitting point binding to the cysteine sulfur atom. In order to simulate the formation of a covalent bond between

the ruthenium atom of the docked RAPTA complexes and the S atom of Cys29, a distance constraint of 2.00 Å (minimum) − 2.60 Å (maximum) was applied between these two atoms centered around an average Ru−S distance of 2.20−2.40 Å.[56] A van der Waals radius of 0.7 Å was used for the Ru(II) ion, and then that of the Cys29 S atom was reduced to 1.50 Å to allow full compatibility with the distance constraints. All the other parameters were used as Gold default values, and the complexes were submitted to 10 genetic algorithm runs using the GOLDScore fitness function.

Acknowledgment. The support and sponsorship by COST Action D39 is kindly acknowledged. A.C. and C.G. thank AIRC for providing them with research grants. T.J.G. thanks the EPFL for financial support, and support from the Swiss National Science Foundation is gratefully acknowledged.

Supporting Information Available: Crystallographic information in CIF format and results from elemental analysis. This material is available free of charge via the Internet at http://pubs.acs.org.

References

(1) Lippert, B. *Cisplatin Chemistry and Biochemistry of a Leading Anticancer Drug*; Wiley: Weinheim, Germany, 1999.
(2) Casini, A.; Hartinger, C.; Gabbiani, C.; Mini, E.; Dyson, P. J.; Keppler, B. K.; Messori, L. Gold(III) compounds as anticancer agents: relevance of gold−protein interactions for their mechanism of action. *J. Inorg. Biochem.* **2008**, *102* (3), 564–575.
(3) Scolaro, C.; Bergamo, A.; Brescacin, L; Delfino, R.; Cocchietto, M.; Laurenczy, G.; Geldbach, T. J.; Sava, G.; Dyson, P. J. In vitro and in vivo evaluation of ruthenium(II)−arene PTA complexes. *J. Med. Chem.* **2005**, *48*, 4161–4171.
(4) Dyson, P. J.; Sava, G. Metal-based antitumour drugs in the post genomic era. *Dalton Trans.* **2006**, 1929–1933.
(5) Williams, C. H., Jr. Thioredoxin−thioredoxin reductase, a system that has come of age. *Eur. J. Biochem.* **2000**, *267*, 6101.
(6) Arnér, E. S. J.; Holmgren, A. Physiological functions of thioredoxin and thioredoxin reductase. *Eur. J. Biochem.* **2000**, *267*, 6102–6109.
(7) Gromer, S.; Urig, S.; Becker, K. The thioredoxin system. From science to clinic. *Med. Res. Rev.* **2004**, *24*, 40–89.
(8) Fritz-Wolf, K.; Urig, S.; Becker, K. The structure of human thioredoxin reductase 1 provides insights into C-terminal rearrangements during catalysis. *J. Mol. Biol.* **2007**, *370* (1), 116–127.
(9) Witte, A. B.; Anestal, K.; Jerremalm, E.; Ehrsson, H.; Arner, E. S. Inhibition of thioredoxin reductase but not of glutathione reductase by the major classes of alkylating and platinum-containing anticancer compounds. *Free Radical Biol. Med.* **2005**, *39*, 696–703.
(10) Coronnello, M.; Mini, E.; Caciagli, B.; Cinellu, M. A.; Bindoli, A.; Gabbiani, C.; Messori, L. Mechanisms of cytotoxicity of selected organogold(III) compounds. *J. Med. Chem.* **2005**, *48*, 6761–6765.
(11) Omata, Y.; Folan, M.; Shaw, M.; Messer, R. L.; Lockwood, P. E.; Hobbs, D.; Bouillaguet, S.; Sano, H.; Lewis, J. B.; Wataha, J. C. Sublethal concentrations of diverse gold compounds inhibit mammalian cytosolic thioredoxin reductase (TrxR1). *Toxicol. in Vitro* **2006**, *20* (6), 882–890.
(12) Marzano, C.; Gandin, V.; Folda, A.; Scutari, G.; Bindoli, A.; Rigobello, M. P. Inhibition of thioredoxin reductase by auranofin induces apoptosis in cisplatin-resistant human ovarian cancer cells. *Free Radical Biol. Med.* **2007**, *42* (6), 872–881.
(13) Mura, P; Camalli, M.; Bindoli, A.; Sorrentino, F.; Casini, A.; Gabbiani, C.; Corsini, M.; Zanello, P.; Rigobello, M. P.; Messori, L. Activity of rat cytosolic thioredoxin reductase is strongly decreased by *trans*-[bis(2-amino-5-methylthiazole)tetrachlororuthenate(III)]: first report of relevant thioredoxin reductase inhibition for a ruthenium compound. *J. Med. Chem.* **2007**, *50* (24), 5871–5874.
(14) Katunuma, N.; Kominami, E. Distributions and localizations of lysosomal cysteine proteinases and cystains. *Rev. Physiol. Biochem. Pharmacol.* **1987**, *108*, 1–20.
(15) Werb, Z. Proteinases and Matrix Degradation. In *Textbook of Rheumatology*; Kelley, W. N., et al., Eds.; W. B. Saunders Co.: Philadelphia, PA, 1989; pp 300−321.
(16) Sloane, B. F.; Moin, K.; Krepela, E.; Rhozhin, J. Cathepsin B and its endogenous inhibitors: the role in tumor malignancy. *Cancer Metastasis Rev.* **1990**, *9*, 333–352.
(17) Koblinski, J. E.; Ahram, M.; Sloane, B. F. Unraveling the role of proteases in cancer. *Clin. Chim. Acta* **2000**, *291* (2), 113–135.
(18) Krueger, S.; Haeckel, C.; Buehling, F.; Roessner, A. Inhibitory effects of antisense cathepsin B cDNA transfection on invasion and motility in a human osteosarcoma cell line. *Cancer Res.* **1999**, *59*, 6010–6014.
(19) Fernandez, P.; Farre, X.; Nadal, A.; Fernandez, E.; Peiro, N.; Sloane, B. F.; Sih, G.; Chapman, H. A.; Campo, E.; Cardesa, A. Expression of cathepsins B and S in the progression of prostate carcinoma. *Int. J. Cancer* **2001**, *95*, 51–55.
(20) Mohanam, S.; et al. Down-regulation of cathepsin B expression impairs the invasive and tumorigenic potential of human glioblastoma cells. *Oncogene* **2001**, *20*, 3665–3673.
(21) Podgorski, I.; Sloane, B. F. Cathepsin B and its role in cancer progression. *Biochem. Soc. Symp.* **2003**, *70*, 263–276.
(22) Chircorian, A.; Barrios, A. M. Inhibition of lysosomal cysteine proteases by chrysotherapeutic compounds: a possible mechanism for the antiarthritic activity of Au(I). *Bioorg. Med. Chem. Lett.* **2004**, *14* (20), 5113–5116.
(23) Mohamed, M. M.; Sloane, B. F. Cysteine cathepsins: multifunctional enzymes in cancer. *Nat. Rev. Cancer* **2006**, *6* (10), 764–775.
(24) Frlan, R.; Gobec, S. Inhibitors of cathepsin B. *Curr. Med. Chem.* **2006**, *13*, 2309–2327.
(25) Mosi, R.; Baird, I. R.; Cox, J.; Anastassov, V.; Cameron, B.; Skerlj, R. T.; Fricker, S. P. Rhenium inhibitors of cathepsin B (ReO (SYS)X (where Y = S, py; X = Cl, Br, SPhOMe-p)): synthesis and mechanism of inhibition. *J. Med. Chem.* **2006**, *49* (17), 5262–5272.
(26) Gunatilleke, S. S.; de Oliveira, C. A.; McCammon, J. A.; Barrios A. M. Inhibition of cathepsin B by Au(I) complexes: a kinetic and computational study. *J. Biol. Inorg. Chem.*, in press.
(27) Gunatilleke, S. S.; Barrios, A. M. Tuning the Au(I)-mediated inhibition of cathepsin B through ligand substitutions. *J. Inorg. Biochem.* **2008**, *102* (3), 555–563.
(28) Gunatilleke, S. S.; Barrios, A. M. Inhibition of lysosomal cysteine proteases by a series of Au(I) complexes: a detailed mechanistic investigation. *J. Med. Chem.* **2006**, *49*, 3933–3937.
(29) Caires, A. C. Recent advances involving palladium(II) complexes for the cancer therapy. *Anticancer Agents Med. Chem.* **2007**, *7* (5), 484–491.
(30) Meloun, B. M.; Baudys, M.; Pohl, J.; Pavlik, M.; Kostka, V. Amino acid sequence of bovine spleen cathepsin B. *J. Biol. Chem.* **1988**, *263*, 9087–9093.
(31) Baudys, M.; Meloun, B.; Gan-Erdene, T.; Pohl, J.; Kostka, V. Disulfide bridges of bovine spleen cathepsin B. *Biol. Chem. Hoppe−Seyler* **1990**, *371*, 485–491.
(32) Scolaro, C.; Chaplin, A. B.; Hartinger, C. G.; Bergamo, A.; Cocchietto, M.; Keppler, B. K.; Sava, G.; Dyson, P. J. Tuning the hydrophobicity of ruthenium(II)−arene (RAPTA) drugs to modify uptake, biomolecular interactions and efficacy. *Dalton Trans.* **2007**, *43*, 5065–5072.
(33) Casini, A.; Mastrobuoni, G.; Ang, W. H.; Gabbiani, C.; Pieraccini, G.; Moneti, G.; Dyson, P. J.; Messori, L. ESI-MS characterisation of protein adducts of anticancer ruthenium(II)−arene PTA (RAPTA) complexes. *ChemMedChem.* **2007**, *2* (5), 631–635.
(34) Ang, W. H.; Daldini, E.; Scolaro, C.; Scopelliti, R.; Juillerat-Jeannerat, L.; Dyson, P. J. Development of organometallic ruthenium−arene anticancer drugs that resist hydrolysis. *Inorg. Chem.* **2006**, *45*, 9006–9013.
(35) Rademaker-Lakhai, J. M.; van den Bongard, D.; Pluim, D.; Beijnen, J. H.; Schellens, J. H. A phase I and pharmacological study with imidazolium-*trans*-DMSO-imidazole-tetrachlororuthenate, a novel ruthenium anticancer agent. *Clin. Cancer Res.* **2004**, *10*, 3717–3727.
(36) Alessio, E.; Mestroni, G.; Bergamo, A.; Sava, G. Ruthenium antimetastatic agents. *Curr. Top. Med. Chem.* **2004**, *4* (15), 1525–1535.
(37) Dorcier, A.; Dyson, P. J.; Gossens, C.; Rothlisberger, U.; Scopelliti, R.; Tavernelli, I. Binding of organometallic ruthenium(II) and osmium(II) complexes to an oligonucleotide: a combined mass spectrometric and theoretical study. *Organometallics* **2005**, *24*, 2114–2123.
(38) Scolaro, C.; Geldbach, T. J.; Rochat, S.; Dorcier, A.; Gossens, C.; Bergamo, A.; Cocchietto, M.; Tavernelli, I.; Sava, G.; Rothlisberger, U.; Dyson, P. J. Influence of hydrogen-bonding substituents on the cytotoxicity of RAPTA compounds. *Organometallics* **2006**, *25*, 756–765.
(39) Dyson, P. J. Systematic design of a targeted organometallic antitumour drug in pre-clinical development. *Chimia* **2007**, *61*, 698–703.
(40) Vock, C. A.; Renfrew, A. K.; Scopelliti, R.; Juillerat-Jeanneret, L.; Dyson, P. J. Influence of the diketonato ligand on the cytotoxicities of $[Ru(\eta^6\text{-}p\text{-cymene})(R2acac)(PTA)]^+$ complexes (PTA = 1,3,5-triaza-7-phosphaadamantane). *Eur. J. Inorg. Chem.* **2008**, *2008* (10), 1661–1671.
(41) Wolohan, P.; Reichert, D. E. CoMSIA and docking study of rhenium based estogen receptor ligand analogs. *Steroids* **2007**, *72*, 247–260.
(42) Rocoux, R.; Bubuc, R.; Dupont, C.; Marechal, J.-D.; Martin, A.; Sellier, M.; Mahy, J.-P. Hemozymes peroxidases activity of artificial hemoproteins constructed from the *Streptomyces lividans* xynalase A and irin(III)-carboxy substituted porphyrins. *Bioconjugate Chem.* **2008**, *19*, 899–910.
(43) Daigle, D. J.; Pepperman, A. B.; Vail, S. L. Synthesis of a monophosphorus analog of hexamethylenetetramine. *J. Heterocycl. Chem.* **1974**, *11*, 407.

(44) Allardyce, C. S.; Dyson, P. J.; Ellis, D. J.; Heath, S. L. [Ru(η6-cymene-p)Cl2(pta)] (pta = 1,3,5-triaza-7-phosphatricyclo[3.3.1.1]decane): a water soluble compound that exhibits pH dependent DNA binding providing selectivity for diseased cells. *Chem. Commun.* **2001**, 1396–1397.

(45) Dyson, P. J.; McIndoe, J. S. Analysis of organometallic compounds using ion trap mass spectrometry. *Inorg. Chim. Acta* **2003**, *354*, 68.

(46) Sheldrick, G. M. *SHELX-97, Structure Solution and Refinement Package*; Universität Göttingen: Göttingen, Germany, 1997.

(47) Bergerhoff, G.; Berndt, M.; Brandenburg, K. Evaluation of crystallographic data with the program DIAMOND. *J. Res. Natl. Inst. Stand. Technol.* **1996**, *101*, 221–225.

(48) Luthman, M.; Holmgren, A. Rat liver thioredoxin and thioredoxin reductase:purification and characterization. *Biochemistry* **1982**, *21*, 6628–6633.

(49) Rigobello, M. P.; Callegaro, M. T.; Barzon, E.; Benetti, M.; Bindoli, A. Purification of mitochondrial thioredoxin reductase and its involvement in the redox regulation of membrane permeability. *Free Radical Biol. Med.* **1998**, *24*, 370–376.

(50) Lowry, O. H.; Rosebrough, N. J.; Farr, A. L.; Randall, R. J. Protein measurement with the Folin phenol reagent. *J. Biol. Chem.* **1951**, *193*, 265–275.

(51) *Maestro Molecular Modeling Interface*, version 5.1.020; Schrodinger, Inc.: Portland, OR.

(52) Becke, A. D. *J. Chem. Phys.* **1993**, *98*, 5648–5652. Becke, A. D *Phys. Rev. A* **1988**, *38*, 3098–3100.

(53) Hay, P. J.; Wadt, W. R. *J. Chem. Phys.* **1985**, *82*, 299–310. Hariharan, P. C.; Pople, J. A *Chem. Phys. Lett.* **1972**, *16*, 217–219.

(54) *Jaguar*, version 6.5; Schrodinger, LLC: New York, 2005.

(55) (a) *GOLD*, version 2.0; Cambridge Crystallographic Data Centre: Cambrigde, U.K.; http://www.ccdc.cam.ac.uk/products/life_sciences/gold/. (b) Jones, G.; Willett, P.; Glen, R. C. Molecular recognition of receptor sites using a genetic algorithm with a description of desolvation. *J. Mol. Biol.* **1995**, *245*, 43–53. (c) Jones, G.; Willett, P.; Glen, R. C.; Leach, A. R.; Taylor, R. Development and validation of a genetic algorithm for flexible docking. *J. Mol. Biol.* **1997**, *267*, 727–748. (d) Verdonk, M. L.; Cole, J. C.; Hartshorn, M. J.; Murray, C. W.; Taylor, R. D. Improved protein−ligand docking using GOLD. *Proteins: Struct., Funct., Genet.* **2003**, *52*, 609–623.

(56) See, for instance, the following: (a) Mashima, K.; Kaneyoshi, H.; Kaneko, S.; Mikami, A.; Tani, K.; Nakamura, A. Chemistry of coordinatively unsaturated bis(thiolato)ruthenium(II) complexes (η^6-arene)Ru(SAr) $_2$ [SAr = 2,6-dimethylbenzenethiolate, 2,4,6-triisopropylbenzenethiolate; (SAr) $_2$ =1,2-benzenedithiolate; arene = benzene, *p*-cymene, hexamethylbenzene]. *Organometallics* **1997**, *16*, 1016–1025, and references therein.

JM8006678